1992-02

Design for an all-reflection Michelson interferometer

Cleary, David D.; Nichols, James W.; Davis, D. Scott

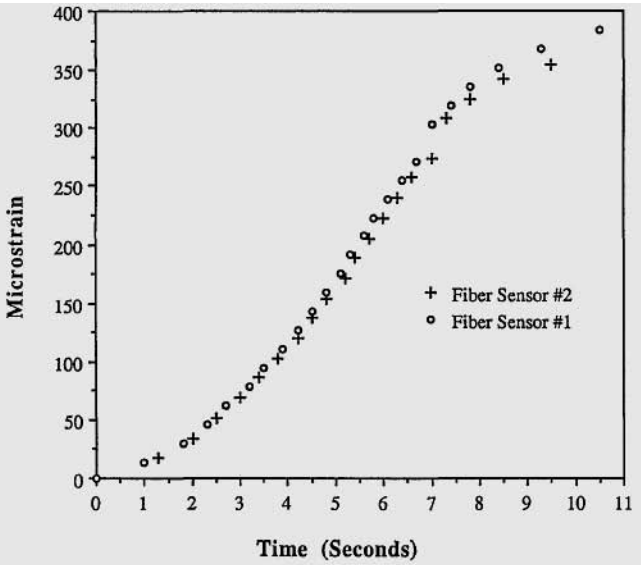

Fig. 3. Data processor output showing the variation of strain versus time. Typical output waveforms shown in Fig. 2 were fed into a software package to acquire strain information at each instant in time.

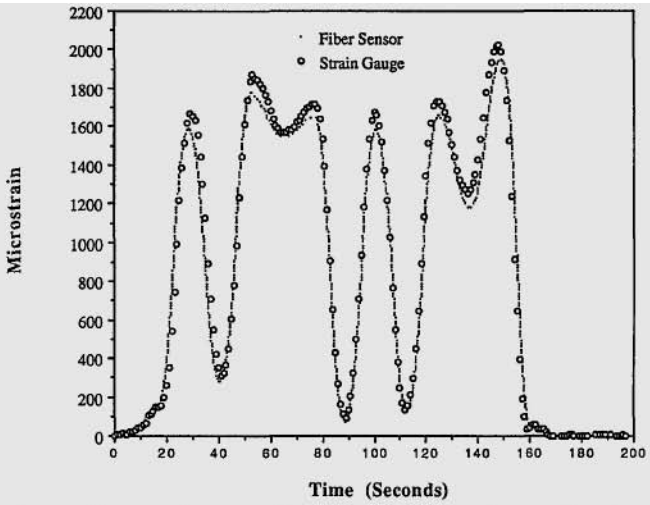

Fig. 4. Processed output showing measured strain as a function of time during the loading cycle.

associated g forces. Strain levels corresponding to the cyclic loading were obtained by using a data acquisition system. Figure 4 shows a comparison of the fiber-sensor output and the electrical strain gauge that was closest to the fiber sensor. The fiber sensor was seen to measure accurately the cyclic loading conditions with a higher resolution than the electrical strain gauges.

We have presented the first results of phase-modulated fiber-optic sensors that were externally adhered to an F-15 aircraft undergoing full-scale fatigue testing. Static and dynamic loading data obtained from the sensors show a high degree of accuracy and a strain resolution of 0.01 μm/m. The use of computerized software for decoding the output fringe pattern and the good agreement with the electrical strain gauges proves the tremendous potential of fiber sensors in practical aerospace and fiber-sensor-based smart structure applications.

We thank Clare A. Paul of the Fatigue, Fracture and Reliability Group, Structural Integrity Branch, and Ken. B. Leger of the Project Engineering Group, Structures Test Branch, for their help with the experiments at Wright Laboratory, Flight Dynamics Directorate, Structures Division, Wright-Patterson Air Force Base, Ohio. This work was supported in part by the Virginia Center for Innovative Technology.

References

1. K. L. Belsley, J. B. Carroll, L. A. Hess, D. R. Huber, and D. Schmadel, "Optically multiplexed interferometric fiber optic sensor system," in *Fiber Optic and Laser Sensors III,* E. L. Moore and O. G. Ramer, eds., Proc. Soc. Photo-Opt. Instrum. Eng. **566,** 257–265 (1985).
2. A. D. Kersey, D. A. Jackson, and M. Corke, "A simple fibre Fabry–Perot sensor," Opt. Commun. **45,** 71–73 (1983).
3. C. E. Lee and H. F. Taylor, "Interferometric optical fibre sensors using internal mirrors," Electron. Lett. **24,** 193–194 (1988).
4. K. A. Murphy, M. F. Gunther, A. M. Vengsarkar, and R. O. Claus, "Quadrature phase shifted extrinsic Fabry-Perot fiber optic sensors," Opt. Lett. **16,** 273–275 (1991).
5. A. M. Vengsarkar and K. A. Murphy, "Fiber sensors in aerospace applications: the smart structures concept," Photonics Spectra **24,** 119–124 (April 1990).

Design for an all-reflection Michelson interferometer

David D. Cleary, James W. Nichols, and D. Scott Davis

The authors are with the Department of Physics, The Naval Postgraduate School, Monterey, California 93943.
Received 1 April 1991.

We present a new design for an all-reflection Michelson interferometer that uses a concave spherical grating in an off-plane Rowland circle configuration.

Key words: *Michelson interferometer, all-reflection.*

Much of our knowledge of the Earth's upper atmosphere has been learned through observations of its ultraviolet spectrum. At low spectral resolution ($\Delta\lambda/\lambda \approx 10^{-2}$) we measure intensities of individual emissions that allow us to investigate atmospheric composition. At moderate resolution ($\Delta\lambda/\lambda \approx 10^{-4}$) we measure Doppler shifts of emission lines that allow us to analyze atmospheric dynamics. At high resolution ($\Delta\lambda/\lambda \approx 10^{-6}$) we can measure the profile of emission lines and investigate the radiation transport of optically thick lines. The latter is confined primarily to the far ultraviolet (FUV) and extreme ultraviolet (EUV) portion of the Earth's atmospheric spectrum.

For space flight observations, high-resolution measurements are made almost exclusively with interferometers rather than spectrometers. Due to the paucity of window materials in the FUV and EUV, Fabry–Perot and standard Michelson interferometers are extremely difficult, if not impossible, to build. As a result, all-reflection interferometers are sought for this portion of the spectrum. A number of designs have appeared in the literature.[1–7] These designs use plane gratings as beam splitters and, in general, require

six reflections for each diffracted beam. In the EUV, where reflectivity can be quite low, it is desired to minimize the total number of reflections. We have designed an all-reflection interferometer that uses a concave grating and requires only three reflections for each path.

The interferometer uses a single Rowland grating for both beam splitting and recombining purposes. A schematic design is shown in Fig. 1. For convenience we define displacements along the Rowland circle with respect to the grating normal by the angle θ. Because the optical elements of this device are placed off-plane from the Rowland circle, we also define displacements above and below the Rowland circle by the angle ϕ. In the current instrument design, the entrance aperture is placed at a horizontal angle θ_{ap} relative to the grating normal and at an angle ϕ_{ap} below the Rowland circle. The diffracted beams for the zero and minus one orders appear at ϕ above the Rowland circle and at the horizontal angles θ_0 and θ_{-1}, respectively. Plane mirrors are placed at the tangential foci for these two beams in order to redirect the light directly back to the grating. Each of these reflected beams generates a zero- and a minus-one-order beam on diffraction from the grating. The twice-diffracted beams recombine, forming an interference pattern across from the entrance at the location $(-\theta_{ap}, \phi_{ap})$. Because each path involves both a zero and minus-one-order diffraction, the intensities of the two beams are equal. Thus fringe contrast is automatically optimized.

The off-plane configuration is necessary to allow the path lengths of the two diffracted beams to be exactly equal. This is important when examining emissions with small coherence lengths (≈ 1 mm). Given that the two mirrors are placed at their respective tangential foci, the two diffracted path lengths will be exactly equal when $-\theta_0 = \theta_{-1}$. It follows that

$$\theta_{ap} = -\theta_{-1}. \tag{1}$$

Assuming that ϕ_{ap} is small, the general grating equation can be used to equate the incident aperture angle θ_{ap} with the negative first-order diffracted beam θ_{-1}. We use standard notation[8] and write

$$\frac{(-1)\lambda}{d} = \sin(\theta_{-1}) - \sin(\theta_{ap}), \tag{2}$$

where (-1) is the order number, λ is the wavelength, and d is the groove spacing. Substitution of Eq. (1) into Eq. (2) yields

$$\theta_{ap} = \sin^{-1}\left(\frac{\lambda}{2d}\right). \tag{3}$$

This gives an expression for the aperture angle in terms of wavelength and the grating characteristics. While the interferometer makes use of only the zero- and negative-first-order beams, in general a grating produces several orders. The efficiency of this device can be optimized by eliminating all but the two required orders with an appropriate choice of θ_{ap}, d, and λ. This is accomplished by ensuring that the angles of the positive-first-order and negative-second-order beams are greater than or equal to 90°. Taking the expression

$$\frac{(1)\lambda}{d} = \sin(\theta_1) - \sin(\theta_{ap}),$$

setting $\theta_1 = 90°$, and solving for θ_{ap} give

$$\theta_{ap} = \sin^{-1}\left(\frac{d-\lambda}{d}\right).$$

We use Eq. (3) to produce the two conditions

$$d = \frac{3\lambda}{2}, \tag{4}$$

$$\theta_{ap} = \sin^{-1}\left(\frac{1}{3}\right) = 19.47°. \tag{5}$$

Equation (4) determines the grating ruling density based on the wavelength of interest, while Eq. (5) gives the incident angle for which the zero- and negative-first-order beams are symmetric about the grating normal. When these two conditions are satisfied, all the incident power will be diffracted into the zero-and minus-one-order beams.

A prototype of this interferometer was constructed using a spherical holographic grating with a radius of curvature of 201.4 mm, a blank diameter of 50 mm, and a ruling density of 1200 lines/mm ($d = 8.3 \times 10^{-7}$ m). For proof of concept, a green He–Ne ($\lambda = 5435$ Å) laser was used as the light source. Note that this combination of wavelength and ruling density does not satisfy Eq. (4) and, as a result, two higher-order beams were present. This, of course, was not significant, given the intensity of a standard He–Ne laser. Figure 2 shows the spatial fringe pattern from this setup recorded on a charge-coupled device (CCD) imager.

The spatial fringes appear as ovals because of the natural astigmatism of the spherical grating. The adaptation of this fringe pattern to a conventional linear array detector may prove to be difficult. However, it appears at the time of this writing that a customized, nonplanar microchannel plate can be fabricated to serve as the detector. Such a device should be able to minimize any nonlinear fringe sampling effects over the narrow spectral ranges that a practical interferometer will employ.

Once a thorough study of the device has been completed, it may turn out that the instrument's off-axis aberrations (astigmatism and coma) will require that the grating and/or

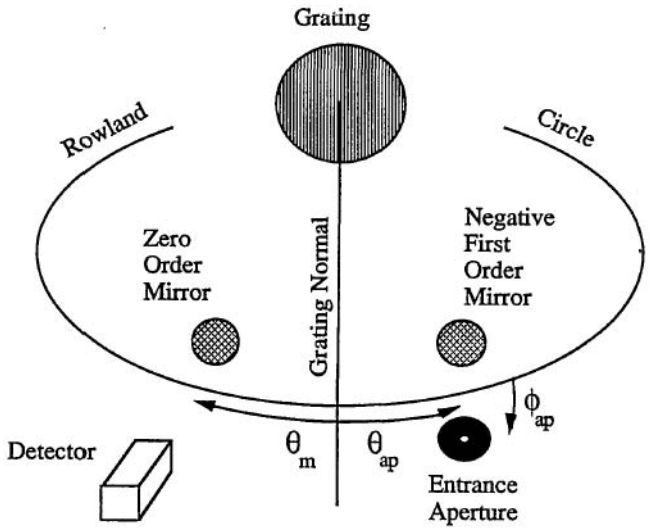

Fig. 1. Schematic diagram of the all-reflection interferometer with entrance aperture, spherical grating, and secondary mirrors shown in three-dimensional perspective.

Fig. 2. Photograph of a typical fringe pattern recorded on a charge-coupled device (CCD) imager.

secondary mirrors be modified. For example, it may be that an elliptical grating or either anamorphic or compound aspheric secondary mirrors will improve system performance. A systematic study of these options is under way. Similarly, because of the astigmatic nature of the system, it is not yet clear whether the proposed device can be configured for different spectral passbands by a simple repositioning of the two secondary mirrors or whether a more complex scheme will be necessary. These issues are currently being studied as well.

This work was sponsored by the Office of Naval Research and the Naval Postgraduate School.

References

1. R. A. Kruger, L. W. Anderson, and F. L. Roesler, "All-reflection interferometer for use as a Fourier-transform spectrometer," J. Opt. Soc. Am. **62,** 938–945 (1972).
2. R. A. Kruger, L. W. Anderson, and F. L. Roesler, "New Fourier transform all-reflection interferometer," Appl. Opt. **12,** 533–540 (1973).
3. B. Chang, R. Alferness, and E. N. Leith, "Space-invariant achromatic grating interferometers: theory," Appl. Opt. **14,** 1592–1600 (1975).
4. R. J. Fonck, D. A. Huppler, F. L. Roesler, D. H. Tracy, and M. Daehler, "All-reflection Michelson interferometer: analysis and test for far IR Fourier spectroscopy," Appl. Opt. **17,** 1739–1747 (1978).
5. Y. Cheng, "Fringe formation in incoherent light with a two-grating interferometer," Appl. Opt. **23,** 3057–3059 (1984).
6. J. Wu, L. Chen, and Y. Jiang, "Imaging 2-D objects with a grating interferometer: two methods," Appl. Opt. **29,** 1225–1229 (1990).
7. J. Harlander, F. L. Roesler, and S. Chakrabarti, "Spatial heterodyne spectroscopy: a novel interferometric technique for the FUV," Tech. Rep. 15, Earth and Planetary Atmospheres Group (University of California, Berkeley, Berkeley, Calif., 1990).
8. M. Born and E. Wolf, *Principles of Optics* (Pergamon, Oxford, 1984), p. 403.

Modified technique for calibrating Fabry–Perot interferometers

T. M. Herbst and S. Beckwith

T. M. Herbst is with the Institute for Astronomy, University of Hawaii, 2680 Woodlawn Drive, Honolulu, Hawaii 66822. When this study was performed, S. Beckwith was with the Department of Astronomy, Cornell University, Ithaca, New York 14853. He is now with the Max-Planck-Institut für Astronomie, Königstuhl, D-6900 Heidelberg 1, Germany.

Received 29 April 1991.
0003-6935/92/040435-05$05.00/0.

We describe a modification to an optical technique to calibrate the cavity spacing of a Fabry–Perot interferometer.

The absolute wavelength calibration of a Fabry–Perot interferometer (FP) is critical to its use as a fixed filter in astronomical observations. Herbst and Beckwith (Paper 1)[1] describe a technique for calibrating and stabilizing the cavity spacing of an infrared FP by using a visible light laser. In this Technical Note we present a refinement to the calibration process that permits setting the central wavelength anywhere within its operating range with high absolute accuracy.

The active stabilization system relies on fringes that are created when a diverging cone of He–Ne laser light passes through the FP at an oblique ($\sim 10°$) angle. These fringes fall upon a pair of position sensitive detectors (PSD's) that return the location of the center of light to the control computer. As the cavity spacing changes the fringes move across the PSD's. The computer calculates the difference between the actual and desired fringe locations and varies the voltages on the piezoelectric actuators in the etalon until this difference is zero. By measuring the fringe locations at the wavelengths of several spectral lines, it is possible to determine the cavity spacing. Since the FP operates at near-infrared wavelengths (1.5–5 μm), the spacing must change by many wavelengths of the He–Ne laser (0.6328 μm).

This is not the classic case of a FP illuminated by collimated light that is subsequently focused in the image plane (see, for example, Born and Wolf[2]). The laser light diverges from a microscope objective, passes through the interferometer, and falls directly on the detectors. This Technical Note examines the fringe formation process and derives a method for determining the absolute wavelength of transmission of the FP.

Figure 1 is a schematic diagram of the optical layout. Laser light diverges from point A, passes through the FP, and falls upon the detectors at D. Adding all rays arriving at D with the appropriate amplitude and phase will give the irradiance at the PSD's. Figure 1 shows two such rays: one passes directly through the FP, while the other suffers two